Fourier Features for Explosive Hazard Detection using a Wideband Electromagnetic Induction Sensor

Brendan Alvey, Alina Zare, Dominic K. C. Ho

ABSTRACT

Sensors which use electromagnetic induction (EMI) to excite a response in conducting bodies have been investigated for the purpose of detecting buried explosives. In particular, wide band EMI sensors which use a relatively low number of operating frequencies have been used to discriminate between types of objects, and to detect objects with very low metal content.[1] In this paper, Fourier features are extracted using the 2D Fourier transform from the complex data; both spatially, and across operating frequencies. Then, the Multiple Instance Adaptive Coherence Estimator (MI-ACE)[2] is used to learn cross-validated target signatures from these features. These signatures, as well as learned background, statistics are used with ACE to generate confidence maps, which are clustered into alarms. Alarms are scored against a ground truth and compared to other detection algorithms.

Keywords: ACE, Adaptive Coerence Estimator, Detection, Electromagnetic Induction, Explosives, Features, Fourier, Hazards, Landmines, MIACE, MIL, Multidimensional Fourier, Multiple Instance, Remote Sensing, WEMI, Wideband

1. INTRODUCTION

A prototype wideband electromagnetic induction (WEMI) sensor has been developed and investigated in the literature for buried explosive object detection and discrimination.[3–10] In this paper, Fourier features are extracted from data collected using this sensor. The Multiple-Instance ACE algorithm is used to learn a target Fourier feature, which is then used with the ACE detector to identify buried explosives.

1.1 Background on the WEMI Sensor

Electromagnetic induction (EMI) sensors typically emit electromagnetic radiation via a transmit coil. This radiation causes metallic elements below the sensor to generate their own induced electromagnetic fields. The electromagnetic response is then picked up by one or more receive coils on the sensor. The specific EMI sensor we considered in the study here is Wideband and operates over twenty-one, logarithmically-spaced frequencies from 330Hz to 90.03KHz.[3] Each sample collected by this sensor is stored as a twenty-one dimensional complex vector which represents the phasor difference between the emitted and the received signals at each of the operating frequencies. The WEMI sensor is attached to a cart, which also has GPS sensors attached to it, to record the UTM spatial coordinates corresponding to each sample.

The data measured by the sensor is filtered in time and space by convolving it with a zero-mean sine filter, as described in (Scott, 2008).[3] This filtering has at least four benefits. First, the ground response is attenuated by differencing nearby sections of ground. For similar reasons, the drift in the system is also mostly removed by this filtering. In addition, the filter has the effect of averaging nearby points which increases the signal to noise ratio. Lastly, the filtered data has a maximum response directly over targets, rather than a minimum due to the geometry and positioning of the coils in this particular sensor. In addition, after sine filtering, the data is uniformly down-sampled in time and space so that each sample is about 1cm from the previous sample.

2. FOMIACE

The Fourier transform is, perhaps, one of the most powerful tools in signal processing. An interpretation of the transform is to look at it as a change of basis from impulses in time, to sinusoidal waves of various frequencies. An advantage of applying the transform is that some functions can be more compactly represented and more easily understood after the change of basis. In a simple case, a perfect sinusoid can be represented by just a frequency and amplitude, instead of with an infinite amount of samples in the time domain. Samples are collected in time

from the EMI sensor. Feature vectors are extracted by simply applying the 2D Fourier transform to the filtered data, with the operating frequency and space as the two dimensions.

Over ground with no targets or clutter there is typically low amplitude, seemingly random noise. Near a metallic target, there is a large increase in the magnitude of the response across most of the operating frequencies. This can be interpreted as a large low frequency component of the signal. If we consider the response across operating frequencies of the sensor, we can exploit a sinusoidal basis as well. Across operating frequencies, background noise tends to be less correlated than over a target. In the frequency domain, a DC signal will show up if all operating frequency responses are identical and nonzero. Other sinusoidal patterns are also present, but more complicated, such as damped ringing effects. A more detailed description of the method used and the specific theories associated are given below.

2.1 Discrete Fourier Transform

The Discrete Time Fourier Transform (DFT) given by equation (1) converts a sequence of equally-spaced samples in time into a sequence of samples equally spaced in the frequency domain. It is one of the basic tools by which frequency analysis is possible. Given N data points with amplitudes denoted, a_n, the transform computes the amplitude of the harmonic components, $\boldsymbol{X}_k$, at N discrete frequencies $2\pi k/N$. To account for phase mismatches, both sine and cosine are used and encoded as a complex-valued number.

$$\boldsymbol{X}_k = \sum_{n=0}^{N-1} a_n e^{\frac{-j2\pi kn}{N}} \tag{1}$$

$$= \sum_{n=0}^{N-1} a_n \Big(cos\Big(\frac{-2\pi kn}{N}\Big) + jsin\Big(\frac{-2\pi kn}{N}\Big)\Big) \tag{2}$$

Typically due to periodicity of the transform, $k = 0, 1, ..., N-1$. A Fast Fourier Transform (FFT) implementation allows for quick computation of the DFT. It is often used to compute the spectrogram of a signal, which displays its frequency information over time. The power spectrum estimate can be computed as $\|\boldsymbol{X}_k\|^2$. While developing the 2D Fourier features, it was first helpful to examine the spectrogram of a single operating frequency of EMI data. Figure 1 shows that targets and background have distinctly different spatial frequency profiles. A window size of 51 samples, which covers a space of approximately 0.51m, was used.

2.2 Two Dimensional Fourier Features

The 1D-DFT, which takes in a sequence of numbers, is constrained to the analysis of one dimensional signals. As mentioned before, there may be frequency information to exploit if we consider the dimension of operating frequencies, in addition to just the spatial dimension. Earlier, it was mentioned that we could examine an instant in time and examine how the response varies, as a function of the 21 operating frequencies of the sensor. Performing the 21-point DFT on this would likely reveal some information. However, what may be more insightful is to look at a collection of these functions in the windows of space used for the spectrogram, shown previously.

By applying the 2D Fourier transform, we are able to extract frequency information from both spacial and operating frequency dimensions. This information is no longer interpreted like strings vibrating, but now more like drum heads vibrating. By incorporating information across both of these dimensions, the dimensionality of a target signature increases by a factor of the spacial window size. The 2D-DFT is given by equation (3).

$$\boldsymbol{X}_{k_1,k_2} = \sum_{m=0}^{M-1} \sum_{n=0}^{N-1} a_{m,n} e^{-j2\pi(k_1 \frac{n}{N} + k_2 \frac{m}{M})} \tag{3}$$

As with the 1D-DFT, optimized fast algorithms allow for a quick multidimensional Fourier analysis. A window of filtered data can be represented as a complex-valued matrix, $\boldsymbol{A}_{M\times N}$, where M is the number of operating frequencies and N is the number of contiguous samples in the window. As with the 1D-DFT, N was set to 51 samples, covering a spatial window of approximately 0.51m. The coefficients can be computed in MATLAB using

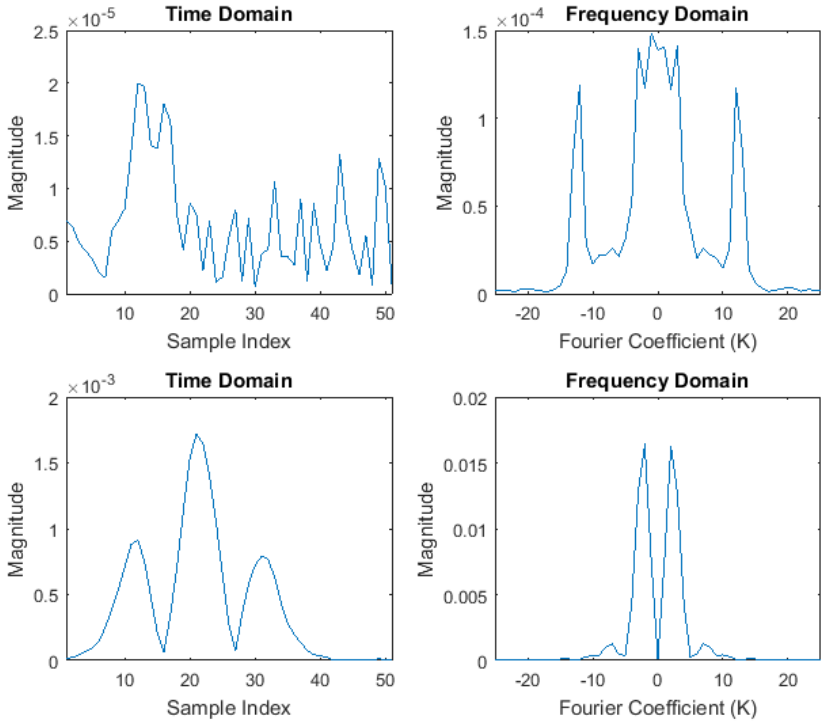

Figure 1. A single operating frequency (number 10) and 1D-DFT is shown. Top Left: Background noise, filtered data, time domain. Top Right: Magnitude of the DFT of background noise. Bottom Left: Metallic target, filtered data time domain. Bottom right: Magnitude of the DFT of the metallic target signal.

$\boldsymbol{X} = fft2(\boldsymbol{A})$. The magnitude of the coefficients are computed and scaled between 0 and 1 for each window. The same target and background samples which were shown using the 1D-FFT are shown using the 2D-FFT in Figure 2. An example of a low-metal target and another background window are given in Figure 3. Because it is difficult to discern merely a true DC shift from low frequency components of the signal, especially across operating frequencies, the DC frequency component is removed. This helps to make the features more robust.

2.3 Multiple-Instance Feature Learning

The 2D Fourier features described above have a strong physical basis. However, modeling an expected 2D Fourier response and creating an ideal target signature with which to do detection is not trivial. Instead, we opt to automatically learn 2D Fourier target features from the data using a Multiple Instance dictionary learning method. The method used, known as Multiple Instance ACE (MIACE), has been specifically tailored for use with the ACE detector. This method was used because, unlike other MIL methods, it has a closed form solution.

2.3.1 MI-ACE

Multiple Instance Learning (MIL) methods can learn target concepts from imprecisely-labeled data.[11–13] In the context of landmine detection, data is often imprecisely labeled. In the case of the WEMI data investigated in this paper, ground truth centroid locations were provided for targets and clutter. However, given only centroids, it is difficult to assign accurate labels to every sample collected. A more intuitive labeling would be to say, somewhere near the ground truth point, there is likely to be a target. This more closely resembles multiple-instance models.

The Adaptive Coherence/Cosine Estimator (ACE) has been shown to be an effective detection statistic.[14–18] ACE assumes that a target data sample can be modeled as a linear combination of a known target signature corrupted by random Gaussian noise. The WEMI sensor being investigated is likely to return data that closely matches this model. ACE uses an estimate of the background mean and background covariance to whiten the

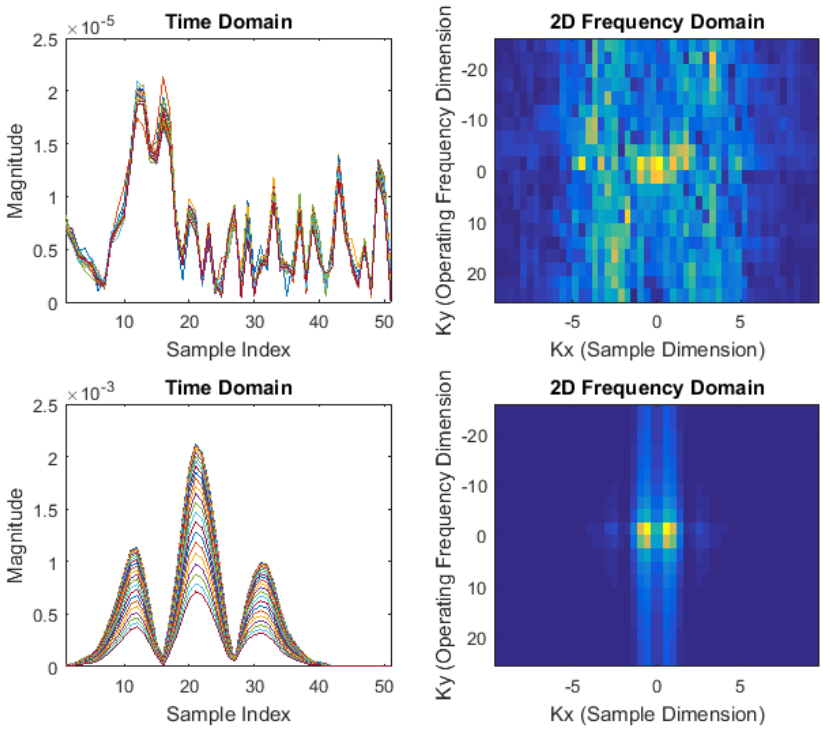

Figure 2. All operating frequencies are used, and the 2D-FFT. Top Left: Background noise, filtered data, time domain. Top Right: Magnitude of the DFT of background noise. Bottom Left: Metallic target, filtered data time domain. Bottom right: Magnitude of the DFT of the metallic target signal.

coordinate space before comparing a known target vector to a data sample using the cosine similarity measure. The ACE detector can be written as equation (4), where $\boldsymbol{s}$ is a known target signature and $\boldsymbol{x}_i$ is a feature vector. The background is assumed to be a Gaussian distribution parametrized by $\boldsymbol{\mu}_b$ and $\boldsymbol{\Sigma}_b$, which represent the mean and covariance, respectively. Geometrically, ACE can be interpreted as the square of the cosine of the angle between $\boldsymbol{x}_i$ and $\boldsymbol{s}$, in a coordinate space whitened by the background estimation.[19]

$$D_{ACE}(\boldsymbol{x}_i, \boldsymbol{s}) = \frac{\boldsymbol{s}^T \boldsymbol{\Sigma}_b^{-1}(\boldsymbol{x}_i - \boldsymbol{\mu}_b)}{\sqrt{\boldsymbol{s}^T \boldsymbol{\Sigma}_b^{-1} \boldsymbol{s}} \sqrt{(\boldsymbol{x}_i - \boldsymbol{\mu}_b)^T \boldsymbol{\Sigma}_b^{-1}(\boldsymbol{x}_i - \boldsymbol{\mu}_b)}} \tag{4}$$

Following from the final ACE equation, an objective function and its updates have been derived to learn a target concept, $\boldsymbol{s}$, from a set of training examples. The training examples are grouped into bags. Each bag is given either a positive or negative label. Positive bags contain at least one target instance. Negative bags contain only background instances. The objective function for MIACE and its update are given in (Zare, 2016).[2] One of the primary advantages of MIACE over some other MIL algorithms is that it has a closed-form solution, allowing for relatively quick learning of new target concepts. Once a target concept is learned, it is then used with the ACE detector.

Previously, ACE and other detectors have been investigated for explosive hazard detection.[19] These detectors have had considerable success using a dictionary generated from an electromagnetic model, known as the Discrete Spectrum of Relaxation Frequencies (DSRF).[10,20] The DSRF generates the expected frequency response of the sensor to metallic objects, which is used as a target concept for a detector. The 2D Fourier features described above are not in the same domain as the DSRF dictionary. Therefore, a new target concept is needed to make use of these features. We combine the use of these 2D Fourier features with learning a target concept using

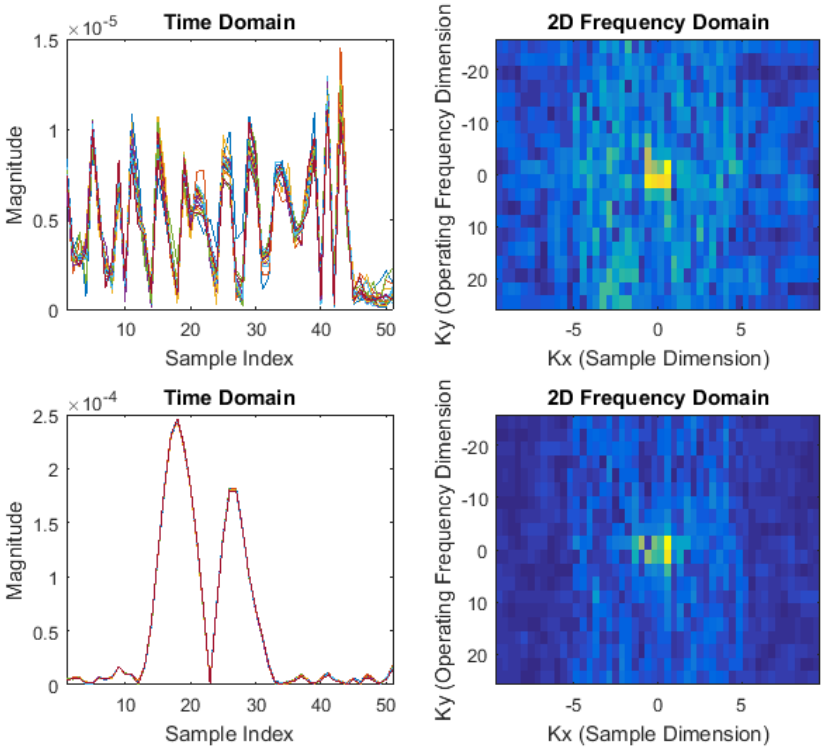

Figure 3. All operating frequencies are used, and the 2D-FFT. Top Left: Background noise, filtered data, time domain. Top Right: Magnitude of the DFT of background noise. Bottom Left: Low-Metal target, filtered data time domain. Bottom right: Magnitude of the DFT of the low-metal target signal.

MIACE in an algorithm we call FOMIACE. The 2D Fourier features and target concepts are vectorized to match the MIACE model.

FOMIACE operates as a prescreener with a sliding window with maximum spatial overlapping. Each window contains 51 spatial samples, each 21 dimensional. The magnitude of the 2D-FFT coefficients are computed and scaled between 0 and 1, after removal ofthe DC frequency components. The coefficients are vectorized, forming a single feature vector, $\boldsymbol{x}_i$, for each window. For each lane, l, a target concept, $\boldsymbol{s}_l$, was learned using lane-based cross-validation. Each window's confidence, $D_{ACE}(\boldsymbol{x}_i, \boldsymbol{s})$, is computed and assigned to the location of the window's spatial center.

3. EXPERIMENTAL RESULTS

3.1 Data Set Description

Experiments were performed on wideband electromagnetic induction data collected at a test facility. The data set consists of fourteen subsets. Each subset contains data from a physical lane where explosive hazards were buried. The cart holding the WEMI system is driven down each of these lanes while collecting WEMI data. With each WEMI data sample, a UTM coordinate is recorded from the on-board GPS system and stored in a header file. The data set consists of a wide variety of explosive hazards, as well as metal and non-metal clutter. The targets were buried at various depths and can be classified by their metallic content and purpose. Object purposes include anti-tank (AT) and anti-personnel (AP). The metallic content of the data set is summarized in Table 1.

3.2 Alarm Generation

Once a confidence map is computed, alarms are generated. Alarms are points of interest, at a certain spatial location, which are marked for further analysis or scoring. Alarms group one or more samples into a single point

Table 1. Metallic Content for WEMI data. Abbreviations, MT: Metal Target, LMT: Low-Metal Target, NMT: Non-Metal Target, CL: Clutter.

	MT	**LMT**	**NMT**	**CL**
Lane 1	4	7	0	6
Lane 2	4	10	0	4
Lane 3	4	7	0	8
Lane 4	6	6	3	0
Lane 5	7	5	5	0
Lane 6	6	6	2	3
Lane 7	0	17	0	0
Lane 8	7	4	3	2
Lane 9	5	7	6	1
Lane 10	7	5	4	2
Lane 11	8	7	5	1
Lane 12	1	6	0	9
Lane 13	6	4	0	5
Lane 14	6	5	0	5
Totals	71	96	28	46

location. This reduces the false alarm rate (FAR) by not scoring every single instance. A mean shift algorithm[21] with a radial basis kernel was used to group data points into alarms for scoring. For each feature vector, $\boldsymbol{x}_i$, FOMIACE is used to compute a confidence, c_i. The associated UTM location is denoted as $\boldsymbol{p}_i$. The mean confidence of points originally within 0.25m of a converged location is used as the final alarm confidence. The width of the kernel, σ, was set to 0.05. The converged threshold, τ, was set to 1cm. The pseudocode for the mean shift algorithm used is shown in Algorithm 1.

Algorithm 1 Mean Shift

for $j = 1$ to I **do**
  ${}^{t-1}\boldsymbol{p}'_j \leftarrow \boldsymbol{\infty}$
  ${}^{t}\boldsymbol{p}'_j \leftarrow \boldsymbol{p}_j$
  while $\|{}^{t}\boldsymbol{p}'_j - {}^{t-1}\boldsymbol{p}'_j\| > \tau$ **do**
    $\forall i : w_i(\boldsymbol{p}'_j) \leftarrow \dfrac{c_i exp\left(-\frac{1}{2}\frac{\|(\boldsymbol{p}'_j - \boldsymbol{p}_i)\|^2}{\sigma}\right)}{\sum_{i'=1}^{I} c_{i'} exp\left(-\frac{1}{2}\frac{\|(\boldsymbol{p}'_j - \boldsymbol{p}_{i'})\|^2}{\sigma}\right)}$
    ${}^{t-1}\boldsymbol{p}'_j \leftarrow {}^{t}\boldsymbol{p}'_j$
    ${}^{t}\boldsymbol{p}'_j \leftarrow \sum_{i=1}^{I} w_i(\boldsymbol{p}'_j)\boldsymbol{p}_i$
  end while
end for

The points start out approximately uniformly distributed approximately 0.1cm apart from each other. As the algorithm iterates, each point moves toward its closest local maxima. Figure 4 shows an example where each sample is alternately updated to show the progress. The final positions of points are at local maxima in the confidence map.

3.3 Experimental Results

The following Receiver Operator Curves (ROCs) were generated using scoring software provided with the WEMI data set. Multiple hits on the same target are not counted as false alarms, through a circular halo of radius 0.25m centered at the target. When hits are scored, polygonal convex hulls surrounding target centroids are computed, taking into account target size and the scoring radius. These polygonal ground truths were extracted from the scoring software by sending every instance in a data lane through scoring as if each point was an alarm. These ground truths were then processed to generate bag labels for each instance. Bag labels, along with the 2D

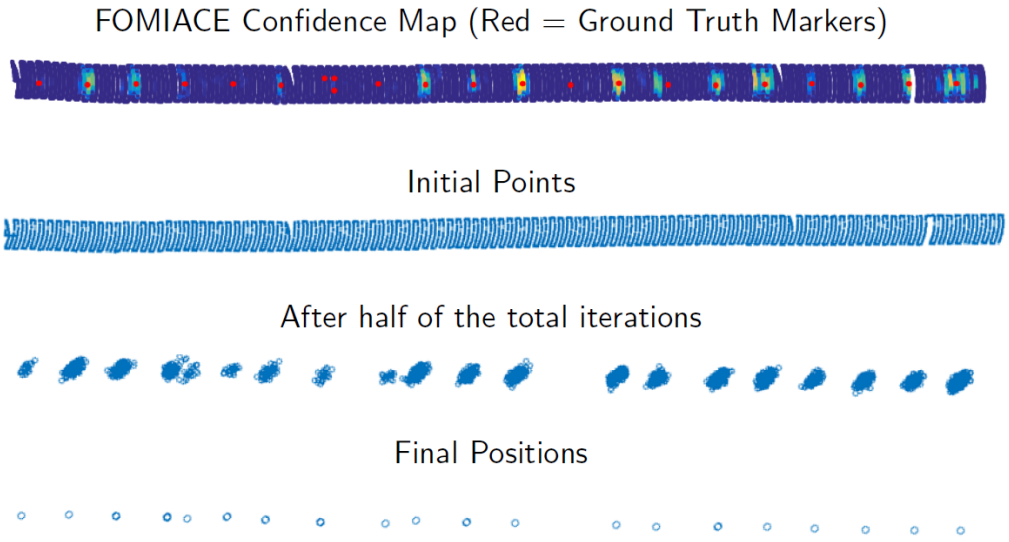

Figure 4. Mean Shift graphical example. Top: FOMIACE confidence map. Not all ground truth markers are targets.

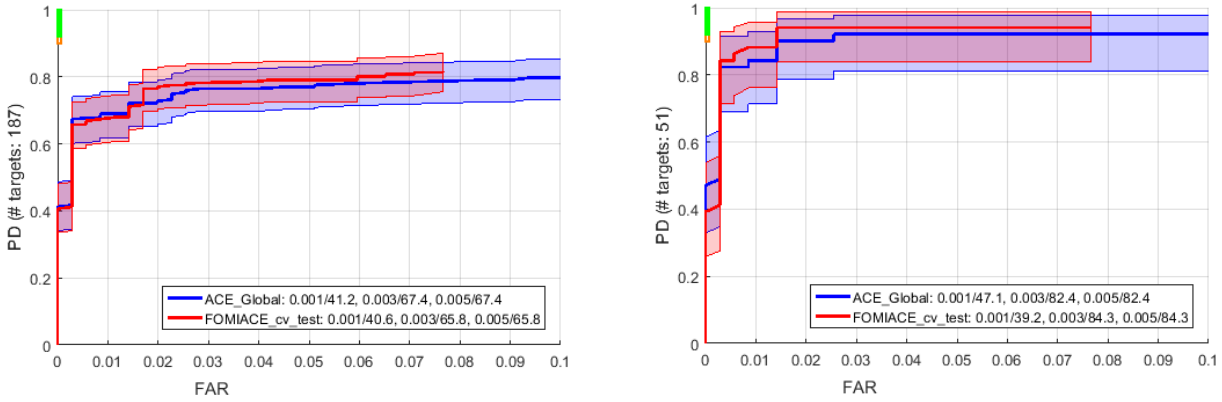

Figure 5. Receiver operator curves comparing FOMIACE to ACE Global over fourteen lanes of WEMI data. Scored on targets up to a depth of 8" with a halo radius of 0.25m. Hits on clutter are ignored. Left, scored on all targets. Right, scored on low-metal AP targets only.

Fourier features were fed into the MIACE algorithm to learn a target Fourier concept. A cross-validation scheme was used whereby 1 subset was left out and tested on, using the other 13 to learn the target concept. These target concepts were used with ACE for detection. Results are compared to ACE with a global background estimate, ran on the sine-filtered data using a 100 element DSRF dictionary. The ROCs of running lane-based cross-validation FOMIACE on the EMI test set are shown in Figure 5.

3.4 Conclusion

The results of the 2D Fourier features look promising. The FOMIACE algorithm, introduced herein, provides a small increase in ROC performance. However, the results are generally within error bars. A qualitative comparison between an ACE confidence map[19] and a FOMIACE confidence map show that FOMIACE, likely due to its inherent windowing, is smoothed a little spatially. This may help to increase signal to noise ratio. It should be noted that ACE is using the 100 element DSRF dictionary, while FOMIACE is only using a single target concept, yet performance is comparable. In addition, should hardware changes be made to the sensor which affect the accuracy of the DSRF dictionary, new target concepts can quickly be learned from new data

using MIACE. Further investigation into higher-dimensional Fourier features, which take into account multiple spatial dimensions, in addition to operating frequencies, could yield further benefits. Likewise, an extension to learn multiple target concepts for both detection and discrimination may improve results.

ACKNOWLEDGMENTS

Research funded by ARO grant number 66398CS to support the US Army RDECOM CERDEC NVESD.

REFERENCES

[1] Tantum, S., Scott, W., Morton, K., Collins, L., and Torrione, P., "Target classification and identification using sparse model representations of frequency-domain electromagnetic induction sensor data," *IEEE Transactions on Geoscience and Remote Sensing* **51**, 2689–2706 (May 2013).

[2] Zare, A., Jiao, C., and Glenn, T., "Multiple instance hyperspectral target characterization," *CoRR* **abs/1606.06354** (2016).

[3] Scott, W., "Broadband array of electromagnetic induction sensors for detecting buried landmines," *IEEE International Geoscience and Remote Sensing Symposium* **2**, 375–378 (2008).

[4] Gao, P., Collins, L., Garber, P., Geng, N., and Carin, L., "Classifcation of landmine-like metal targets using wideband electromagnetic induction," *IEEE Transactions on Geoscience and Remote Sensing* **38**, 1352–1361 (2000).

[5] Dula, J., Zare, A., Ho, K. C., and Gader, P., "Landmine classifcation using possibilistic k-nearest neighbors with wideband electromagnetic induction data," *SPIE Proceedings* **8709**, 87091 (2013).

[6] Yuksel, S., Ramachandran, G., Gader, P., Wilson, J., Ho, K. C., and Heo, G., "Hierarchical methods for landmine detection with wideband electromagnetic induction and ground penetrating radar multisensor systems," *IEEE International Geoscience and Remote Sensing Symposium* **2**, 177–180 (2008).

[7] Ramachandran, G., Gader, P., and Wilson, J., "GRANMA: Gradient angle model algorithm on wideband emi data for landmine detection," *IEEE Geoscience and Remote Sensing Letters* **7**, 535–539 (2010).

[8] Gao, P., Collins, L., Geng, N., and Carin, L., "Classifcation of buried metal objects using wideband frequency domain electromagnetic induction responses: a comparison of optimal and sub optimal processors," *IEEE International Geoscience and Remote Sensing Symposium* **3**, 1819–1822 (1999).

[9] Goldberg, S., Glenn, T., Wilson, J., and Gader, P., "Landmine detection using two-tapped joint orthogonal matching pursuits," *SPIE Proceedings* **8357**, 83570B–83570B–8 (2012).

[10] Wei, M.-H., Scott, W., and McClellan, J., "Landmine detection using the discrete spectrum of relaxation frequencies," *IEEE International Geoscience and Remote Sensing Symposium* , 834–837 (2011).

[11] Jiao, C. and Zare, A., "Functions of multiple instances for learning target signatures," *IEEE Transactions on Geoscience and Remote Sensing* **53**, 4670–4686 (Aug 2015).

[12] Maron, O. and Lozano-Pérez, T., "A framework for multiple-instance learning," in [*Advances in Neural Information Processing Systems 10*], Jordan, M. I., Kearns, M. J., and Solla, S. A., eds., 570–576, MIT Press (1998).

[13] Bolton, J. and Gader, P., "Application of multiple-instance learning for hyperspectral image analysis," *IEEE Geoscience and Remote Sensing Letters* **8**, 889–893 (Sept 2011).

[14] Kraut, S., Scharf, L., and Butler, R., "The adaptive coherence estimator: a uniformly most powerful invariant adaptive detection statistic," *IEEE Transactions on Signal Processing* **53**, 427–438 (2005).

[15] Yan, H., Zhang, Y., Wei, W., Zhang, L., Li, F., and Wang, B., "An mcd based local ace algorithm for hyperspectral imagery target detection," *IEEE International Conference on Orange Technologies* , 21–24 (2014).

[16] Scharf, L. and McWhorter, L., "Adaptive matched subspace detectors and adaptive coherence estimators," *Signals Systems and Computers Conference Record of the Thirtieth Asilomar Conference* **2**, 1114–1117 (1996).

[17] McWhorter, L., Scharf, L., and Grifths, L., "Adaptive coherence estimation for radar signal processing," *Signals Systems and Computers Conference Record of the Thirtieth Asilomar Conference* **1**, 536–540 (1996).

[18] Manolakis, D., "Detection algorithms for hyperspectral imaging applications: a signal processing perspective," *IEEE Workshop on Advances in Techniques for Analysis of Remotely Sensed Data* , 378–384 (2003).

[19] Alvey, B., Zare, A., Cook, M., and Ho, K. C., "Adaptive coherence estimator (ace) for explosive hazard detection using wideband electromagnetic induction (wemi)," *Proc. SPIE* **9823**, 982309–982309–7 (2016).

[20] Wei, M.-H., Scott, W., and J., M., "Robust estimation of the discrete spectrum of relaxations for electromagnetic induction responses," *IEEE Transactions on Geoscience and Remote Sensing* **48**, 1169–1179 (2010).

[21] Comaniciu, D. and Meer, P., "Mean shift: a robust approach toward feature space analysis," *IEEE Transactions on Pattern Analysis and Machine Intelligence* **24**, 603–619 (May 2002).